Journal of Luminescence 205 (2019) 277–281

Contents lists available at ScienceDirect

Journal of Luminescence

journal homepage: www.elsevier.com/locate/jlumin

An investigation on the luminescence quenching mechanism of $ZnGa_2O_4:Tb^{3+}$ phosphor

T.A. Safeera, E.I. Anila*

Optoelectronic and Nanomaterials' Research Laboratory, Department of Physics, U C College, Aluva, Kerala 683102, India

ARTICLE INFO

Keywords:
Oxide spinel
Microrods
Quenching
Green phosphor

ABSTRACT

Rod like green emitting $ZnGa_2O_4:Tb^{3+}$ phosphor were synthesized and the effect of Tb^{3+} on the structural and optical properties of zinc gallate were analysed. Cubic spinel nature of $ZnGa_2O_4:Tb^{3+}$ nano crystallite was verified from the x-ray diffraction. From the photoelectron spectroscopy analysis, chemical states of constituent elements were identified. Photoluminescence spectra reveal the green emission quenching and there are no reports about this mechanism from $ZnGa_2O_4:Tb^{3+}$ phosphor synthesized via solid state reaction route. Quadrupole – quadrupole interaction leads to this quenching behaviour and the critical distance is 21 Å.

1. Introduction

The diversity in applications exhibited by zinc gallium oxide (zinc gallate-$ZnGa_2O_4$) such as in field emission displays, electroluminescent devices, photocatalyst, water splitting etc lead researchers to produce more stable and attractive forms of this inorganic oxide [1–3]. Also,the good optical transparency and conductivity features direct its applications in liquid crystal displays and in solar cells [4,5]. It is a cubic spinel with Zn^{2+} and Ga^{3+} ions possessing tetrahedral and octahedral coordination respectively, with a small inversion in site occupancy [6]. The wide bandgap of 4.4 eV helps this spinel oxide for better performance in various applications. Doping with Mn^{2+} or Tb^{3+} gives rise to green emission, whereas Cr^{3+} or Eu^{3+} doping leads to red emission [6–9].

Among the various methods of preparation, such as thermal evaporation [10], pulsed laser ablation [11], sol-gel [9], hydrothermal [12] etc, we employed the most common method for the synthesis of long lasting phosphor material, which is the solid state reaction method. Authors have already reported a comparative study of ZnO, Ga_2O_3 and $ZnGa_2O_4$ using this method [13]. The increased number of defects produced by the high sintering temperature leads to the afterglow shown by gallates, which is the advantage of using this method.

Rare earth doping in oxides have much interest in recent studies because of their enhanced optical properties emerged by the shielding effect produced by the outer orbit electrons. Here we report the synthesis of $ZnGa_2O_4$ doped with the lanthanide, terbium (Tb^{3+}) ion by solid state reaction method. Effect of Tb^{3+} concentration on the properties of $ZnGa_2O_4$: Tb^{3+} phosphor is rarely reported. Also there are no reports on the formation of $ZnGa_2O_4:Tb^{3+}$ rods as obtained in this work. This phosphor is well known with its green emission resulting from $^5D_4$–$^7F_5$ transition [7]. The f-f transitions responsible for this emission produce narrow, sharp photoluminescence emissions. There exists a quenching behaviour in PL spectra, due to the multipolar interaction, which induce energy transfer between the Tb^{3+} ions.

2. Experimental

The samples were synthesized by solid state reaction method, where the required metal oxides such as Zinc oxide [ZnO, 99%, MERCK] and Gallium oxide [Ga_2O_3, 99.99%, ALDRICH] were homogenously mixed together with terbium nitrate [Tb $(NO_3)_3$, Sigma, 99.9%] using 2-propanol. After drying, the samples were annealed at a temperature of 1000 °C for 12 h. The detailed synthesis procedure is given in our previous report [13]. Samples were prepared for different doping concentrations of terbium. The final powder after sintering was ground using mortar and pestle and used for characterization.

Bruker AXS D8 advance x-ray diffractometer was used for the analysis of phase and structural parameters, by x-ray diffraction (XRD) technique. Scanning electron microscopy (SEM) was employed for morphological study using TESCAN VEGA 3 SBH. Thermo Scientific K-ALPHA X-ray photoelectron spectroscopy (XPS) was employed for the analysis of elemental composition and chemical states of the synthesized sample. The diffuse reflection for the bandgap determination was recorded using Varian, Cary 5000 UV–VIS–NIR Spectrophotometer. Horiba Flouromax-4C Spectrofluorometer was used for the determination of various defects and the emission behaviour in the synthesized

* Corresponding author.
E-mail address: anilaei@gmail.com (E.I. Anila).

https://doi.org/10.1016/j.jlumin.2018.09.033
Received 11 January 2018; Received in revised form 12 September 2018; Accepted 14 September 2018
Available online 15 September 2018

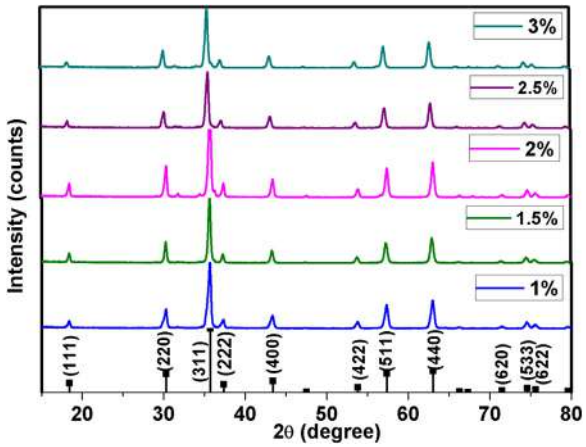

Fig. 1. X-ray diffraction pattern of $ZnGa_2O_4$:Tb^{3+} for different molar concentrations of Tb^{3+}.

Table 1
Variation in lattice constants with molar concentration of Tb^{3+} ion.

Tb^{3+} molar concentration (%)	Lattice parameter (A°)	Grain size (nm)
Bulk	8.336	–
1	8.342	20
1.5	8.345	25
2	8.359	24
2.5	8.377	28
3	8.38	20

sample using photoluminescence (PL) study.

3. Results and discussions

The x-ray diffractogram showing the major reflections of Tb^{3+} doped zinc gallate is represented in Fig. 1. Although there is a broadening due to the size effect, XRD exhibits the well crystalline and pure nature of synthesized zinc gallium oxide. All the diffraction peaks agree with the same JCPDS, having file no. 86–0415 keeping spinel cubic structure with fd3m spacegroup. With the incorporation of Tb^{3+} ion, there is a shift to the lower angle side compared to the JCPDS. The peak shift increases with the activator concentration and it is noticeable for 2.5 and 3 mol%. This shift is due to the high ionic radius of the dopant Tb^{3+} ion (92 pm) compared to the host Ga^{3+} ion (76 pm), which causes an increase in lattice parameter values (Table 1).

The crystallite size of the samples were calculated using the Scherrer formula (relation 1), which connects grain size (D) with x-ray wavelength (λ), full width at half maximum (β) and glancing angle (θ) and the obtained values are in the range 20–30 nm.

$$D = \frac{0.9\lambda}{\beta \cos\theta} \quad (1)$$

There is an expression relating interplanar distance (d_{hkl}) with lattice parameter (a) and miller indices [*hkl*], which can be utilized for the determination of lattice constants (Eq. (2)).

$$d_{hkl} = \frac{a}{\sqrt{h^2 + k^2 + l^2}} \quad (2)$$

The calculated crystallite size and lattice parameter values with molar concentration of Tb^{3+} is arranged in Table 1.

Fig. 2 represents the SEM and TEM micrographs of the sample with 2.5 mol% of Tb^{3+}. SEM reveals the one dimensional growth of $ZnGa_2O_4$:Tb^{3+} phosphor (Fig. 2a). From the TEM image also (inset of Fig. 2b) we can confirm this rod like nature of the phosphor. The HRTEM image of the micro rod which exhibits the crystal lattice planes is shown in Fig. 2b. These 1D structures have improved optoelectronic applications [14]. The SAED pattern showing the electron diffraction from a selected area, with lattice planes (111) and (220) is represented in Fig. 2c. This type of spot pattern is a peculiarity of rod like structures.

SEM images of Tb^{3+} doped zinc gallate for varying doping concentrations is portrayed in Fig. 3. There is no observable change in the micrographs with varying Tb^{3+} concentration. All exhibit clustered rod like behaviour having micro length.

The chemical state identification of $ZnGa_2O_4$:Tb^{3+} phosphor was done by XPS technique and the corresponding spectra is as shown in Fig. 4. The survey spectra of $ZnGa_2O_4$:Tb^{3+} consist of binding energy peaks corresponding to Zn 2p, Ga 2p, Ga 3d, O 1s and Tb 3d elemental states as shown in Fig. 4.1. A binding energy peak representing C 1s (~284.6 eV) element is observable from the spectra, which is meant for the charge correction while taking XPS [15]. The fine spectra for each constituent elements, which indicate their chemical states are portrayed in Fig. 4(2)–4(6). The variation in peak energy values with molar concentration of dopant ion, for individual elemental species of $ZnGa_2O_4$:Tb^{3+} is recorded in Table 2. The formation of zinc gallate spinel is established from energy separation (ΔE) between Zn $2p_{3/2}$ and Ga $2p_{3/2}$ values which is ~96 eV [16]. The energy peak at 530 eV confirms the presence of O^{2-} ion in zinc gallate [17]. The energy difference between Zn $2p_{3/2\text{-}1/2}$ and Ga $2p_{3/2\text{-}1/2}$ for $ZnGa_2O_4$:Tb^{3+} are given in Table 2, which are comparable with the standard values of 22.97and 26.84 eV respectively which confirms the bonding of Zn^{2+} and Ga^{3+} with O^{2-} [15,18,19]. The 3d state of Ga^{3+} is responsible for the peak around 20 eV [20]. The fine spectra of Tb^{3+} in $ZnGa_2O_4$:Tb^{3+} is shown in Fig. 4(6), and the peak corresponds to the 3d chemical state with a total angular momentum value of 3/2 [21].

$ZnGa_2O_4$:Tb^{3+} exhibits almost 90% diffuse reflectance over the visible region of the DRS spectra, and it is almost identical for all activator concentrations (Fig. 5a). Also, there exists an absorption band in the UV region around 370 nm which arise from the intra-$4f^8$ transitions ie $4f^8$ to $4f^7 5d$ transition of Tb^{3+} ion [22].

From the reflectance (R) values, band gap values can be estimated by making use of Kubelka-Munk relation (Eq. (3)), which connects R with absorption (k) and scattering (s) coefficients [23,24]. Fig. 5b represents the Tauc plot of $ZnGa_2O_4$:Tb^{3+} phosphor for different activator concentrations. The calculated bandgap values are recorded in

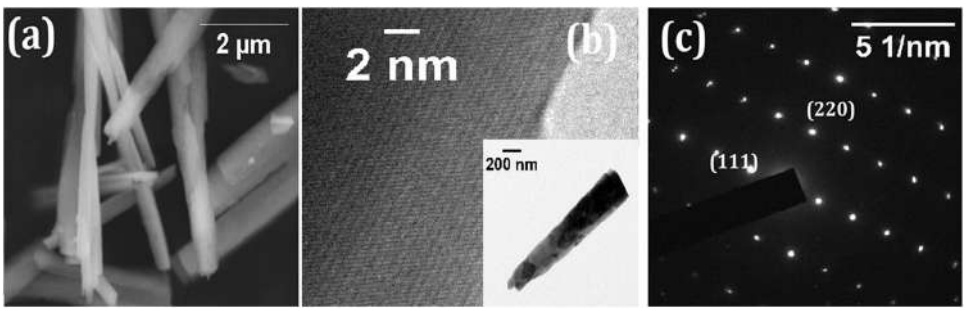

Fig. 2. (a) SEM, (b) HRTEM and TEM [inset] images and (c) SAED pattern of $ZnGa_2O_4$:Tb^{3+} phosphor for 2.5 mol% Tb^{3+} concentration.

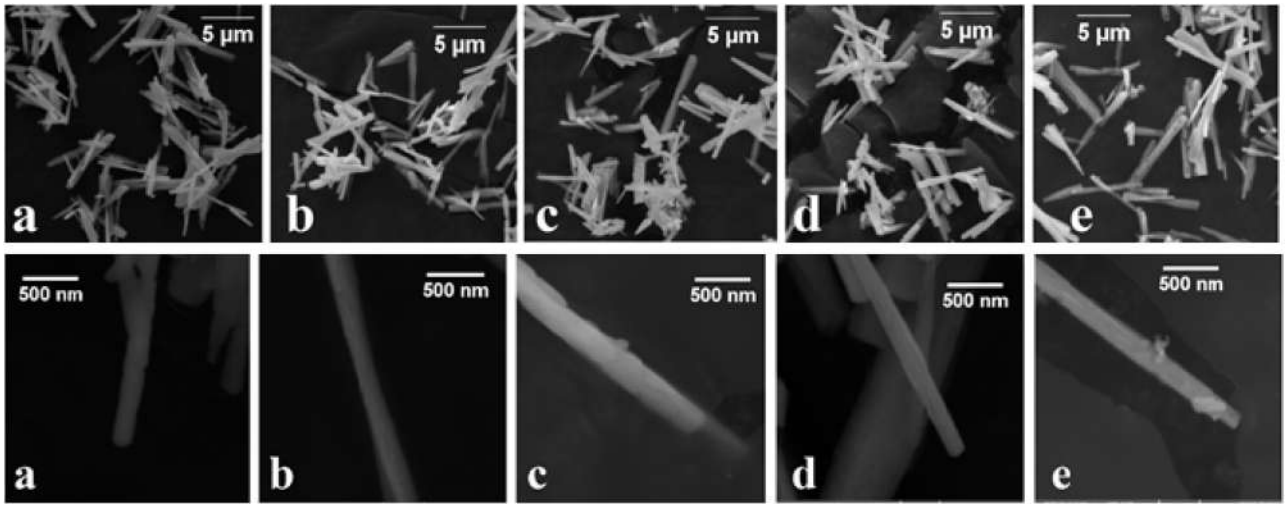

Fig. 3. (a) SEM images of $ZnGa_2O_4$:Tb^{3+} phosphor with varying molar concentrations of Tb^{3+} [a, b, c, d and e denotes 1, 1.5, 2, 2.5 and 3 mol% doped samples respectively].

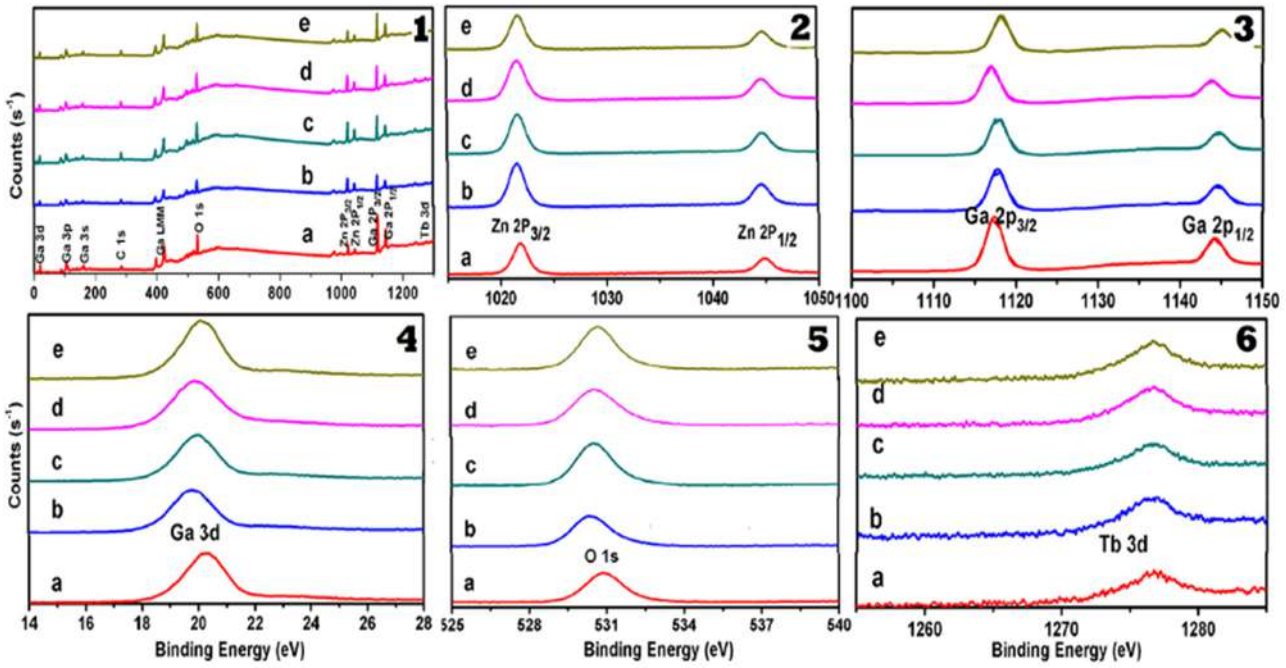

Fig. 4. (1) XPS survey spectra and fine spectra of (2) Zn 2p, (3) Ga 2p, (4) Ga 3d, (5) O1 s & (6)Tb 3d of $ZnGa_2O_4$:Tb^{3+} for different doping concentrations [a, b, c, d and e denotes 1, 1.5, 2, 2.5 and 3 mol% respectively].

Table 2
Effect of Tb^{3+} incorporation on binding energy of $ZnGa_2O_4$:Tb^{3+} phosphor.

Chemical state	Binding energy (eV)				
	1%	1.5%	2%	2.5%	3%
Zn $2p_{3/2}$	1021.78	1021.46	1021.62	1021.68	1021.73
Zn $2p_{1/2}$	1044.87	1044.61	1044.77	1044.63	1044.82
Ga $2p_{3/2}$	1117.39	1117.71	1117.80	1116.86	1118.24
Ga $2p_{1/2}$	1144.56	1144.63	1143.83	1144.88	1145.04
Ga 3d	20.29	19.80	20.01	19.92	20.11
O 1s	530.93	530.34	530.53	530.54	530.69
Tb 3d	1276.66	1276.55	1276.58	1276.68	1276.75
Energy separation, ΔE (eV)					
Zn 2p $_{(3/2\text{-}1/2)}$	23.09	23.15	23.15	22.95	23.09
Ga 2p $_{(3/2\text{-}1/2)}$	27.17	26.92	26.03	28.02	26.8

Table 2.

$$\frac{k}{s} = \frac{(1-R)^2}{2R} \quad (3)$$

The grain size as well as band gap are varying with doping concentration but not in a specific order. Fig. 5c represents the crystallite size and band gap variations with molar concentrations of Tb^{3+}. Defects in the samples produce band tails which reduces the band gap whereas higher carrier concentration will increase the band gap (B M shift) [25,26]. These two factors, band tails and BM shift may be causing the small fluctuations in band gap.

The photoluminescence behaviour of $ZnGa_2O_4$:Tb^{3+} phosphor is depicted in Fig. 6a. On exciting with a wavelength of 290 nm, intense emissions with peaks at 490 and 547 nm were observed. They are attributed to the characteristic emission lines of activator Tb^{3+} ion. The first peak around 490 nm is due to $^5D_4 \rightarrow {}^7F_6$ transition and the one at

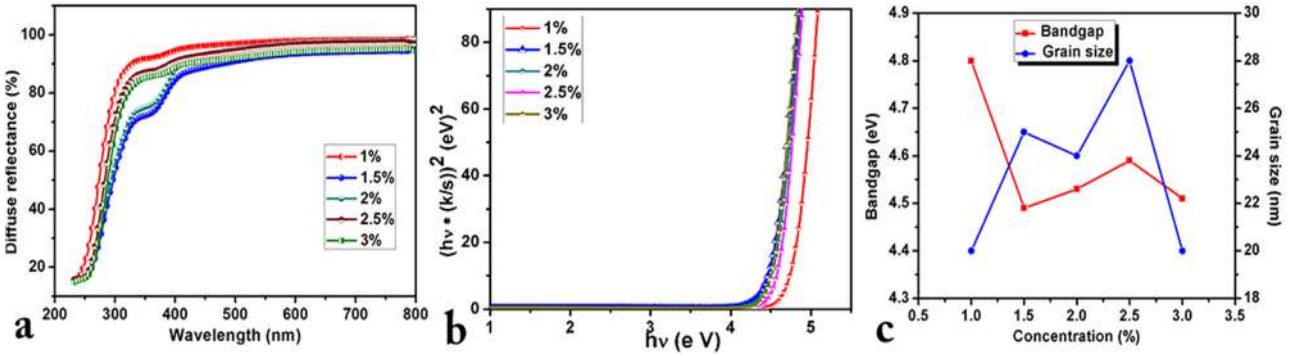

Fig. 5. (a) Diffuse reflectance spectra, (b) Tauc plot and (c) variation of band gap and crystallite size of $ZnGa_2O_4:Tb^{3+}$ phosphor with mol% Tb^{3+}.

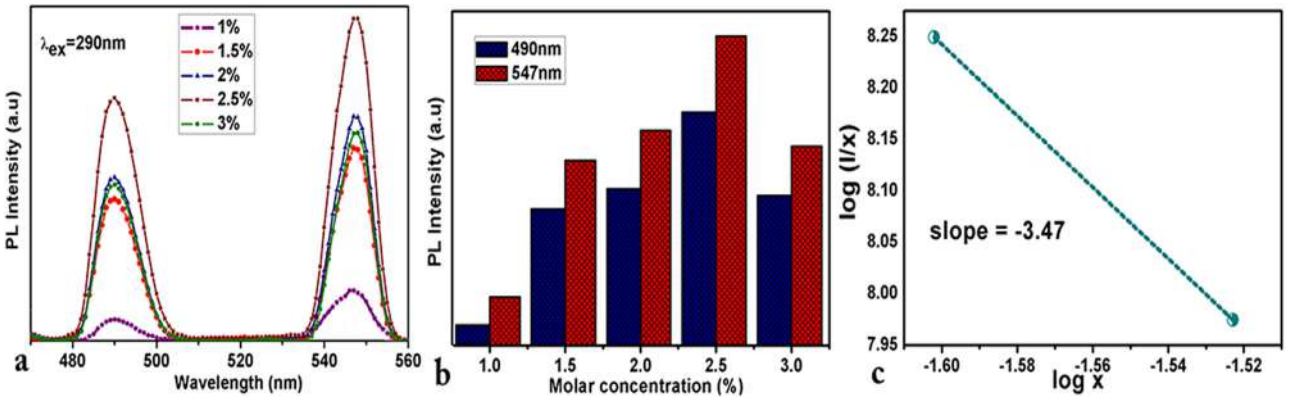

Fig. 6. (a) Photoluminescence spectra, (b) peak intensity variation and (c) log(x) vs log(I/x) graph of $ZnGa_2O_4:Tb^{3+}$ phosphor with different concentrations of Tb^{3+}.

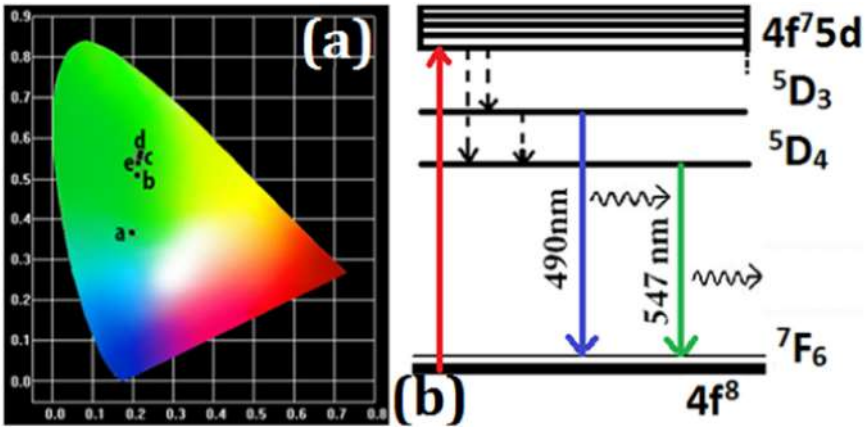

Fig. 7. (a) CIE chromaticity diagram and (b) energy band diagram for $ZnGa_2O_4:Tb^{3+}$ phosphor [a to e represents 1–3 M concentration of Tb^{3+} and - - represents the nonradiative emissions].

Table 3
Variation in optical parameters with molar concentration of Tb^{3+} ion.

Molar concentrations of Tb^{3+} (%)	Band gap (eV)	CIE coordinates	
		x	y
1	4.8	0.20	0.37
1.5	4.49	0.21	0.51
2	4.53	0.22	0.55
2.5	4.59	0.22	0.56
3	4.51	0.21	0.54

547 nm is assigned to $^5D_4 \rightarrow {}^7F_5$ electronic transition [7,22,27]. Spectroscopic studies shows that the type of transitions $^5D_4 \rightarrow {}^7F_5$ and $^5D_4 \rightarrow {}^7F_6$ is electric-dipole and magnetic-dipole respectively. The ratio of intensities of $^5D_4 \rightarrow {}^7F_5$ to $^5D_4 \rightarrow {}^7F_6$ also known as green to blue luminescence ratio is a good parameter to find out the extent of distortion in the crystal lattice. Thus the PL analysis can be used for the determination of asymmetry in local environment around Tb^{3+} ion as reported in the case of Eu^{3+} and Dy^{3+} ions [27–30].

With increase in Tb^{3+} concentration, the PL intensity of its characteristic emissions also increases upto 2.5% and then decreases (Fig. 6b). At higher concentrations, the reduction in spacing between the dopant ions and its pairing leads to the probability of cross relaxation, hence quenching of emission intensity. The given excitation energy is transferred between the dopant ions (Tb^{3+}) and promote quenching of green emission. The critical distance (R_c), which is the shortest distance between dopant ions to bring about the concentration quenching can be calculated using the expression [31]:

$$R_c \approx 2\left[\frac{3V}{4X_c\pi Z}\right]^{\frac{1}{3}} \quad (4)$$

where V = volume of unit cell = 582.18 Å^3, Z = 5, number of cations per unit cell, X_c = critical concentration after which quenching begins = 0.025. So the critical distance for Tb^{3+} ions in $ZnGa_2O_4$:Tb^{3+} is evaluated to be 21 Å.

The restricted distance for exchange interaction is about 4 Å, hence no exchange interaction is possible and the energy transfer is achieved by multipolar interaction. Since the Dexter and Van Uitert formulated a relation for finding out the type of multipolar interaction among the activator ions which stimulate the energy tansfer [32,33]. It connects the activator concentration (x) with intensity of emission (I) by the relation;

$$\frac{I}{x} = k\left[1 + \beta[x]^{\frac{Q}{3}}\right]^{-1} \quad (5)$$

where k and β denotes constants of host lattice and Q represents the type of interation. Q = 6,8,10 respectively for dipole-dipole, dipole-quadrapole and quadrapole-quadrapole interactions. It can be estimated from the slope of the log(x) vs log(I/x) graph [Fig. 6.c]. In our case, slope of the graph = -3.46 = -Q/3 ie Q~10, which implies that the multipolar interaction in $ZnGa_2O_4$:Tb^{3+} phosphor which induce the energy tansfer is quadrupole-quadrupole interation.

Commission Internationale de l′ Elcairage (CIE) chromaticity diagram, which is the quantization of PL emission is represented in Fig. 7a. The diagram visually represents the change in color from bluish green to green with the molar concentration of Tb^{3+} ion. The corresponding CIE coordinates are arranged in Table 3.

The various electronic transitions from the Tb^{3+} ion, which are responsible for the characteristic emissions in the PL spectra is also depicted in Fig. 7.b. On exciting with 290 nm, electrons are transferred from $4f^8$, ground state to the $4f^75d$ excited state. From there, electrons are shifted to the $^5D_4$ and $^5D_3$ levels by a non-radiative transition (through phonon interaction) as displayed. From the excited ^5D levels, de-excitation to $^7F_6$ level occurs together with emissions at 490 nm and 547 nm.

4. Conclusions

Green emitting $ZnGa_2O_4$:Tb^{3+} phosphor for different activator concentrations were prepared and their structural and optical properties were analysed with respect to Tb^{3+} molar concentrations. The rod like zinc gallate exhibit concentration quenching behaviour due to quadrupole-quadrupole interaction among the activator ions. The emission color gets shifted from bluish green to green on increasing the terbium concentration. This intense green emission can be made use of in display devices and for imaging purpose in biomedical field.

Acknowledgements

The authors thank Board of Research in Nuclear Sciences (BRNS), Department of Atomic Energy (DAE), India for financial support. T A Safeera thanks University Grants Commission (UGC) for Maulana Azad fellowship.

References

[1] Jin Liu, Wei Lu, Hongzhang Wu, Lin Jin, Bin Hu, Lili Li, Zhenling Wang, In situ synthesis of rice-like $ZnGa_2O_4$ for the photocatalytic removal of organic and inorganic pollutants, Mater. Sci. Semicond. Process. 56 (2016) 251–259.
[2] Musa Mutlu Can, G. Hassnain Jaffari, Seda Aksoy, S. Ismat Shah, Tezer Fırat, Synthesis and characterization of $ZnGa_2O_4$ particles prepared by solid state reaction, J. Alloy. Compd. 549 (2013) 303–307.
[3] Caroline E. Knapp, Joe A. Manzi, Andreas Kafizas, Ivan P. Parkin, Claire J. Carmalt, Aerosol-assisted chemical vapour deposition of transparent zinc gallate films, ChemPlusChem 79 (2014) 1024–1029.
[4] Liangliang Liu, Jianfeng Huang, Liyun Cao, Jianpeng Wu, Jie Fei, Haibo Ouyang, Fenglan Ma, Changjiang Zhou, Synthesis of $ZnGa_2O_4$ octahedral crystallite by hydrothermal method with the aid of CTAB and its photocatalytic activity, Mater. Lett. 95 (2013) 160–163.
[5] H. Xue, Z. Li, L. Wu, Z. Ding, X. Wang, X. Fu, Nanocrystalline ternary wide band gap p-block metal semiconductor $Sr_2Sb_2O_7$: hydrothermal syntheses and photocatalytic benzene degradation, J. Phys. Chem. C 112 (2008) 5850–5855.
[6] Philip D. Rack, Jeffrey J. Peterson, Michael D. Potter, Wounjhang Park, Eu^{+3} and Cr^{+3} doping for red cathodoluminescence in $ZnGa_2O_4$, J. Mater. Res. 16 (2001) 1429–1433.
[7] Zhihua Xu, Yongxiang Li, Zhifu Liu, Dong Wang, UV and X-ray excited luminescence of Tb^{3+}-doped $ZnGa_2O_4$ phosphors, J. Alloy. Compd. 391 (2005) 202–205.
[8] Hiromichi Hayashi, Atsuko Suino, Kenji Shimoyama, Masafumi Takesue, Suguru Tooyama, Richard L. Smith Jr, Continuous hydrothermal synthesis of $ZnGa_2O_4$:Mn^{2+} nanoparticles at temperatures of 300–500∘C and pressures of 25–35 MPa, J. Supercrit. Fluids 77 (2013) 1–6.
[9] T.A. Safeera, E.I. Anila, Synthesis and characterization of $ZnGa_2O_4$:Eu^{3+} nanophosphor by wetchemical method, Scr. Mater. 143 (2018) 94–97.
[10] Xiao Meng Chen, Guang Tao Fei, Jian Yan, Yan Qing Zhu, Li. De Zhang, Synthesis of $ZnGa_2O_4$ hierarchical nanostructure by Au catalysts induced thermal evaporation, Nanoscale Res. Lett. 5 (2010) 1387–1392.
[11] S.S. Yi, I.W. Kim, J.S. Bae, B.K. Moon, S.B. Kim, J.H. Jeong, Luminescence characteristics of $ZnGa_2O_4$ thin film phosphors grown by pulsed laser deposition, Mater. Lett. 57 (2002) 904–909.
[12] Masanori Hirano, Mikimasa Imai, Michio Inagaki, Preparation of $ZnGa_2O_4$ spinel fine particles by the hydrothermal method, J. Am. Ceram. Soc. 83 (4) (2000) 977–979.
[13] T.A. Safeera, N. Johns, K. Mini Krishna, P.V. Sreenivasan, R. Reshmi, E.I. Anila, Zinc gallate and its starting materials in solid state reaction route- a comparative study, Mater. Chem. Phys. 181 (2016) 21–25.
[14] Yong Sheng Zhao, Hongbing Fu, Aidong Peng, Ying Ma, Qing Liao, Jiannian Yao, Construction and optoelectronic properties of organic one-dimensional nanostructures, Acc. Chem. Res. 43 (2010) 409–418.
[15] Musa Mutlu Can, G. Hassnain Jaffari, Seda Aksoy, S. Ismat Shah, Tezer Fırat, Synthesis and characterization of $ZnGa_2O_4$ particles prepared by solid state reaction, J. Alloy. Compd. 549 (2013) 303–307.
[16] L. Zou, X. Xiang, M. Wei, F. Li, D.G. Evans, Single-crystalline $ZnGa_2O_4$ spinel phosphor via a single-source inorganic precursor route, Inorg. Chem. 47 (2008) 1361–1369.
[17] Caroline E. Knapp, Joe A. Manzi, Andreas Kafizas, Ivan P. Parkin, Claire J. Carmalt, Aerosol-assisted chemical vapour deposition of transparent zinc gallate films, ChemPlusChem 79 (2014) 1024–1029.
[18] Yanping Yuan, Weimin Du, Xuefeng Qian, $Zn_xGa_2O_{3+x}$ ($0 \le x \le 1$) solid solution nanocrystals: tunable composition and optical properties, J. Mater. Chem. 22 (2012) 653–659.
[19] J.F. Moulder, W.F. Stick, P.E. Sobol, K.D. Bomben, J. Chanstain, R.C. King Jr. (Eds.), Handbook of X-ray Photoelectron Spectroscopy, Physical Electronics, Inc., USA, 1992.
[20] Mingjia Lu, Xin Ouyan, Songping Wu, Rongyun Ge, Rui Xu, A facile hydrothermal route to self-assembled $ZnGa_2O_4$ particles and their microwave application, Appl. Surf. Sci. 364 (2016) 775–782.
[21] Hongda Li, Wenjun Li, Shaonan Gu, Fangzhi Wang, Hualei Zhou, In-built $Tb4^+$/Tb^{3+} redox centers in terbium-doped bismuth molybdate nanograss for enhanced photocatalytic activity, Catal. Sci. Technol. 6 (2016) 3510–3519.
[22] T.R.N. Kutty, Abanti Nag, Photoluminescence due to efficient energy transfer from Ce^{3+} to Tb^{3+} and Mn^{2+} in $Sr_3Al_{10}SiO_{20}$, Mater. Chem. Phys. 91 (2005) 524–531.
[23] P. Kubelka, F. Munk, Ein Beitragzur Optik der Farbanstriche, Zh. Tekh. Fiz. 12 (1931) 593–601.
[24] P. Kubelka, New contributions to the optics of intensely light-scattering materials, Part 1, J. Opt. Soc. Am. 38 (1948) 448–457.
[25] Piet Van Mieghem, Theory of band tails in heavily doped semiconductors, Rev. Mod. Phys. 64 (1992) 755–793.
[26] E. Burstein, Anomalous optical absorption limit in InSb, Phys. Rev. 93 (1954) 632–633.
[27] A.J. Silversmith, D.M. Boye, K.S. Brewer, C.E. Gillespie, Y. Lu, D.L. Campbell, $^5D_3$-^7F_j emission in terbium doped sol gel glasses, J. Lumin. 121 (2006) 14–20.
[28] Zhihua Xu, Yongxiang Li, Zhifu Liu, Dong Wang, UV and X-ray excited luminescence of Tb^{3+}doped $ZnGa_2O_4$ phosphors, J. Alloy. Compd. 391 (2005) 202–205.
[29] H.X. Zhang, C.H. Kam, Y. Zhou, X.Q. Han, S. Buddhudu, Y.L. Lam, C.Y. Chan, Deposition and photoluminescence of sol-gel derived Tb^{3+}:Zn_2SiO_4 films on SiO_2/Si, Thin Solid Films 370 (2000) 50–53.
[30] L.J. Nugent, R.D. Baybarz, J.L. Burnett, J.L. Ryan, Electron-transfer and f-d absorption bands of some lanthanide and actinide complexes and the standard (II-III) oxidation potential for each member of the lanthanide and actinide series, J. Phys. Chem. 77 (12) (1973) 1528–1539.
[31] G. Blasse, A. Brill, Photo luminescent efficiency of phosphors with electronic transitions in localized centers, J. Electrochem. Soc. 113 (1968) 1067–1075.
[32] D.L. Dexter, A theory of sensitized luminescence in solids, J. Chem. Phys. 21 (1953) 836–850.
[33] D.L. Dexter, J.H. Schulman, Theory of concentration quenching in inorganic phosphors, J. Chem. Phys. 22 (1954) 1063–1070.